sciendo
Austrian Journal of Earth Sciences | Vienna | 2023 | Volume 116 | 1 - 15 | DOI: 10.17738/ajes.2023.0001

# The temporal evolution of seismicity and variability of b-values along the Vienna Basin Transfer Fault System

Asma Nasir[1], Esther Hintersberger[2], Kurt Decker[1]*

[1)] Department of Geology, University of Vienna, Althanstraße 14, A-1090 Vienna, Austria; asma.nasir1100@gmail.com; kurt.decker@univie.ac.at

[2)] Department of Geological Mapping, Geosphere Austria, Neulinggasse 38, 1030 Vienna, Austria; Esther.Hintersberger@geosphere.at

* corresponding author

**KEYWORDS:** Vienna Basin Transfer Fault System, seismicity, aftershock, Gutenberg-Richter relations

**Abstract**

The Vienna Basin Transfer Fault System (VBTFS) is the most active fault system in the region between the Eastern Alps, the western Carpathians and the Pannonian Basin. The spatial and temporal distribution of earthquakes along the fault system shows a heterogeneous pattern including a long-time decay of seismicity at the northern part of the VBTFS, which was interpreted to result from a long aftershock sequence subsequent to the 1906 Dobrá Voda earthquake (M=5.7). In this paper we investigate if other segments of the VBTFS display similar long-term declines of seismicity that might indicate long aftershock sequences following strong, yet unrecorded, earthquakes in historical times.

In order to analyse the distribution of seismicity, the VBTFS is divided into arbitrary segments of about 50 km length each. The segments are chosen to overlap each other to avoid missing information from neighbouring segments due to arbitrarily selected segment boundaries. For each segment we analyse the temporal evolution of seismicity and calculate the parameters of the corresponding Gutenberg-Richter (GR) relation.

The temporal seismicity patterns revealed from the segments covering the Dobrá Voda area confirm the protracted aftershock sequence following the 1906 earthquake. All but one of the other segments do not show temporal changes of seismicity comparable to the long-term Dobrá Voda aftershock sequence. Seismicity patterns, however, include short-term Omori-type aftershocks following moderate earthquakes such as the 2000 Ebreichsdorf earthquake (M=4.8). The segment covering the SW tip of the VBTFS revealed a 200 years long gradual decrease of the largest observed magnitudes starting with the 1794 Leoben (M=4.7) earthquake. The 1794 event is the oldest earthquake listed in the catalogue for the region under consideration. It therefore remains open if the recorded decay of seismicity results from the 1794 event, or a stronger earthquake before that time. The latter is corroborated by the low magnitude of the 1794 earthquake which would typically not be considered to cause long aftershock sequences.

GR a- and b-values, calculated for the individual segments, vary significantly along the VBTFS. Values range from 0.47 to 0.86 (b-values) and 0.81 to 2.54 (a-values), respectively. Data show a significant positive correlation of a- and b-values and a coincidence of the lowest b-values with fault segments with large seismic slip deficits and very low seismicity in the last approximately 300 years. These parts of the VBTFS were previously interpreted as “locked” fault segments, which have a significant potential to release future strong earthquakes, in spite of the fact that historical and instrumentally recorded seismicity is very low. We find this interpretation corroborated by the low b-values that suggest high differential stresses for these fault segments.

## 1. Introduction

The Vienna Basin, a Miocene pull-apart basin between the eastern margin of the Alps and the Carpathian fold-thrust belt, is one of the most seismically active areas in intraplate Europe. The main active fault system is referred to as the Vienna Basin Transfer Fault System (VBTFS), a major, about 380 km long left-lateral strike-slip fault system, that starts from the central Eastern Alps (Mur-Mürz Fault, Gutdeutsch and Aric, 1988; Brückl et al., 2010), crosses the entire pull-apart basin from SW to NE (e.g., Royden, 1985; Wessely, 1988; Kröll and Wessely, 1993; Decker, 1996; Decker et al., 2005; Beidinger and Decker, 2011) and proceeds into the Dobrá Voda area of the Carpathian fold-thrust belt. The fault system is further traced into the area around Žilina in the Váh Valley (Schenková et al., 1995; Gutdeutsch and Aric, 1988; Decker and Peresson, 1996; Sefara et al., 1998).

The spatial distribution of earthquakes along the part of the VBTFS in the Mur-Mürz Valley, the Vienna Basin and the adjacent Brezovské Karpaty shows a peculiar pattern with concentrated activity in the south of the Vienna Basin and an apparent lack of earthquakes in its central and northern part (Fig. 1; Hinsch and Decker, 2003; 2011). Here, we analyze the historical and instrumental records of earthquakes in this region in order to better understand the causes for this heterogeneous distribution.

The spatiotemporal correlation and energy release of earthquake occurrence is complex, but not random (Hainzl et al., 2003). The Gutenberg–Richter law states that the number of earthquakes with magnitude greater or equal to a certain magnitude occurring in a given time decreases logarithmically with increasing magnitude (Gutenberg and Richter, 1942). The gradient of the Gutenberg-Richter (GR) relation, the so-called b-value, is commonly close to 1 in seismically active regions (Scholz, 2002). However, the b-value varies with respect to time,

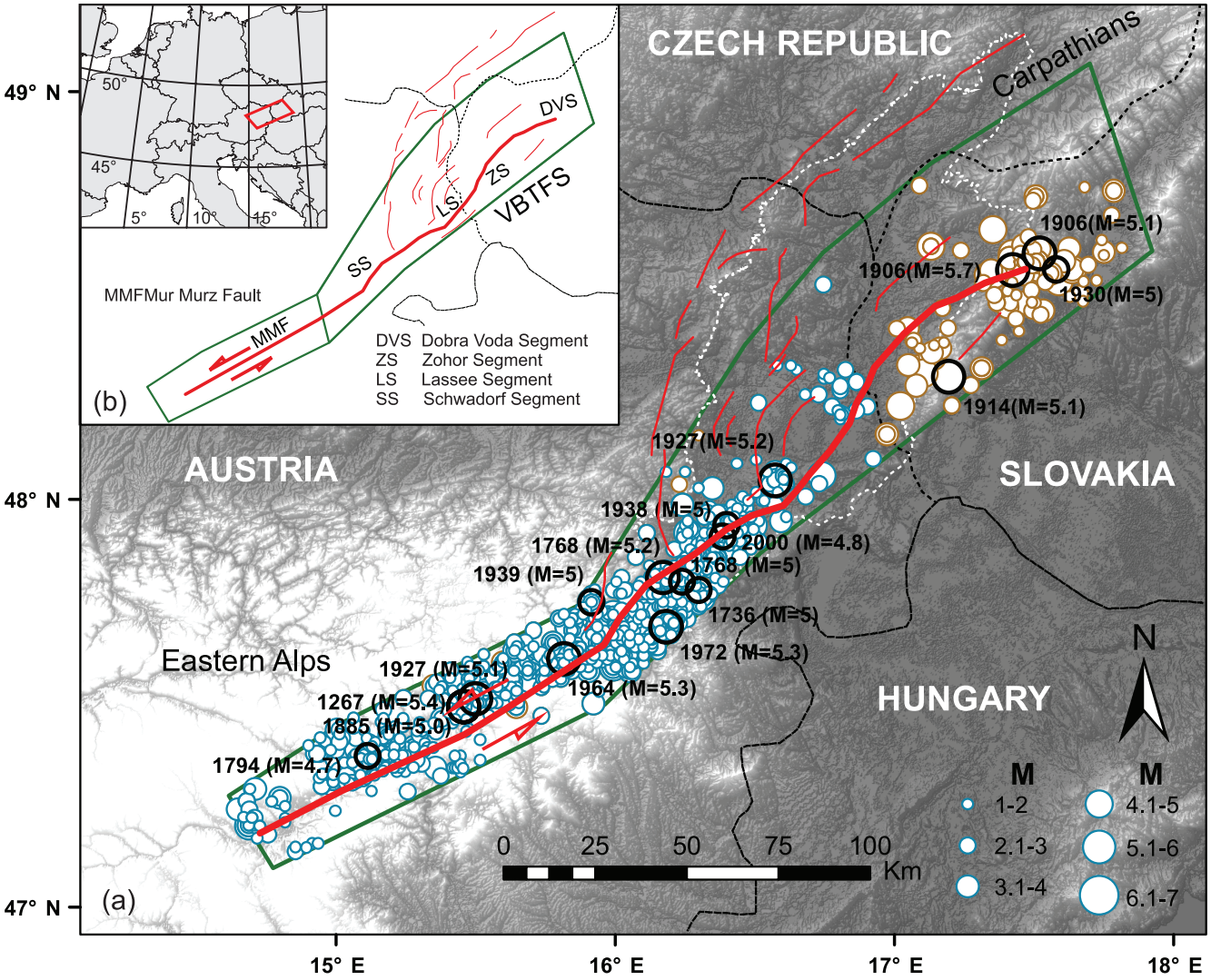


**Figure 1:** (a) Distribution of earthquakes along the Vienna Basin Transfer Fault System (VBTFS). Blue circles show earthquakes from the Austrian earthquake catalogue (ZAMG, 2020), brown circles are earthquakes listed in the ACORN (2004) catalogue. Black circles denote earthquake with M≥5. Green polygon indicates the extent VBTFS. Note the uneven distribution of seismicity with very low seismicity along the Lassee (LS) and Zohor (ZS) segments in the Vienna Basin as well as close to the SW termination of the Mur-Mürz-Fault (MM; see inset (b for location of the named segments). White stippled line marks the outline of the Miocene pull-apart basin. (b) Overview maps showing the extent of the VBTFS and locations of fault segments mentioned in the text.

space, and magnitude ranges, since it is related to earthquake rupture dynamics, or seismic source characteristics (Senatorski, 2019). In addition, the b-value is observed to decrease with stress (Scholz, 1968; 2015). Therefore, Schorlemmer and Wiemer (2004) proposed that spatially varying b-values can be used to forecast future seismicity more accurately than the approach in which one assumes a constant b-value equal to the average regional value.

Another possible cause of the documented heterogeneous earthquake activity might be the occurrence of long aftershock sequences. Aftershock activity is generally triggered by a strong earthquake. In the aftermath of a large earthquake, this aftershock activity leads to a local increase of seismic activity, which later on decays back to a lower level labeled as 'normal' background seismicity (Stein and Liu, 2009). The length of an aftershock sequence can vary from a few months at plate margins to several years and even decades and centuries in intraplate regions (Stein and Liu, 2009), depending not only on the magnitude of the causing earthquake, but apparently also on the regional level of background seismicity and the fault-loading rate. At the northeastern end of the Vienna Basin, the 1906 Dobrá Voda mainshock (M=5.7) has caused elevated seismicity in its near vicinity which is still visible today (Nasir et al., 2020). Therefore, we will check whether the seismic activity on other parts of the VBTFS can be explained as the result of a (pre-)historic strong mainshock.

In this publication, we will address the questions raised above using a newly compiled earthquake catalogue using the data by ZAMG (2020) and ACORN (2004) to cover the whole extent of the VBTFS. As the major part of the 754-years-long earthquake catalogue is based on intensity, we apply an empirical intensity-magnitude conversion formula, which is derived from the catalogues.

## 2. Tectonic setting

The Vienna Basin Transform Fault is an active fault system extending over a distance of some 380 km from the Eastern Alps through the Vienna Basin into the West Carpathians. Active sinistral movement is indicated by moderate seismic activity in a NE striking zone paralleling the fault system, focal plane solutions and recent stress measurements (Decker et al., 2005). The Vienna Basin is regarded as one of the most prominent seismic active regions of Austria (Fig. 1). The pull-apart basin is oriented NE-SW and extends from the Semmering mountain range to the little Carpathians in Slovakia (Gutdeutsch and Aric, 1988). The VBTFS passes between the capitals of Austria (Vienna) and Slovakia (Bratislava), which are situated to the west and to the east of the fault system, respectively.

The VBTFS and the Vienna pull-apart basin started to develop in the Middle Miocene. Extension and basin subsidence initiated in the Badenian (15.5 Ma) as dated by the growth strata of the basin fill (Royden, 1985; Wessely, 1988) and terminated in the Late Miocene (about 7-8 Ma; Peresson and Decker, 1997). Pull-apart basin formation was associated with about 30 km of sinistral displacement along the VBTFS, which corresponds to an average Miocene sinistral slip rate of 4 mm/a (Linzer et al., 2002; Decker et al., 2005). Since then, tectonic movement slowed down to a moderate level of 1-2 mm/a as determined by GPS geodesy (Grenerczy et al., 2000; 2005; see also Möller et al., 2011, for discussion). Umnig et al. (2015) reported a slip rate of 0.35-0.43 mm/a based on a 4-years data series from a local GNSS network. Geological data derived from the age and thickness of Quaternary sediments that accumulated in a Quaternary pull-apart basin (Mitterndorf Basin) indicate a slip rate between 1.5 and 2.6 mm/a (Decker et al., 2005).

Two studies have been carried out to evaluate the seismic energy release of the fault and compare it to geologically and geodetically derived slip rates, considering both, pre-instrumental and instrumental earthquake data (Hinsch and Decker, 2003; 2011). The cited studies revealed significant seismic slip deficits for the VBTFS as a whole, and several fault segments in particular. The largest slip deficits were recorded for the Lassee and Zohor Segments (see Fig. 1 (b) for location) and the SW part of the Mur-Mürz Fault which released virtually no seismic energy in historical times. These parts of the VBTFS were interpreted as currently locked segments.

Earthquakes of magnitude 5 tend to happen on average every 25 years along the VBTFS in the last about 250 years (Fig. 1). The strongest recorded events are the earthquakes of 1267 Kindberg ($I_0$=VIII/M=5.4) and 1907 Dobra Voda ($I_0$=VII-IX/M=5.7). These magnitudes are well below the magnitude of Maximum Credible Earthquakes (MCE) estimated from the length and fault area of geologically defined fault segments by knick points of the strike-slip fault and branchlines of normal faults (Decker and Hintersberger, 2011; Hinsch and Decker, 2011). The latter reveal MCE magnitudes between about M=6.0-6.8 for the different fault segments. The MCE estimates are supported by paleoseismological evidence (Hintersberger et al., 2014).

## 3. Earthquake data

Earthquake catalogues are one of the most important products of seismology. Before any scientific analysis it is necessary to assess the quality, consistency, and homogeneity of the data (Woessner and Wiemer, 2005). As the Vienna Basin is located partly in Austria and Slovakia, two earthquake catalogues have to be considered in order to cover the entire length of the VBTFS. The Austrian earthquake catalog includes both historical and instrumental data from 04.05.1201 to 06.05.2020 having a magnitude range of $M_w$=1-6.1 (ZAMG, 2020). In comparison to an older version that we used in earlier completeness studies (Nasir et al., 2013), one historical earthquake (27.08.1668; M=4.6) at Wiener Neustadt and one instrumental earthquake (05.07.1973; M=0.7) have been removed from the new Austrian earthquake catalogue.

The ACORN (2004) earthquake catalogue covers a rectangular region encompassing the Eastern Alps, West Carpathians, and Bohemian Massif (Czech Republic, Slovakia, Hungary and Austria; Lenhardt et al., 2007b). The temporal span of the ACORN earthquake catalogue is between 1267 to 2004 with a magnitude range from 0.5 to 5.7.

Both, the Austrian earthquake catalogue (ZAMG, 2020) as well as the ACORN earthquake catalogue, are dominated by pre-instrumental earthquake data. Generally, historical earthquake data are reported with intensity, which is then converted into magnitude. For this conversion different formulas and empirical correlations were suggested for countries in Central Europe (Grünthal et al., 2009). The conversion of intensity into magnitude for the Austrian catalogue is obtained by the formula $M= 2/3I_0$ (Lenhardt, 2007a). Conversion for the ACORN earthquake catalogue is given by the following formula (Grünthal et al., 2009).

$$M_w = 0.682I_0 + 0.16 \quad \text{(not considering focal depth)}$$
$$M_w = 0.667I_0 + 0.3\log(h) + 0.1 \quad \text{(considering focal depth)}$$

where h is the focal depth and $I_0$ is the macroseismic intensity.

In the region of the VBTFS, the majority of earthquakes are listed with hypocenter depths up to 10 km. The maximum depth is 35 km. Comparison of both catalogues in the overlapping region (Fig. 2a) shows the effect of the use of different intensity-magnitude conversions. Intensity to magnitude conversions for historical earthquakes for intensities $3 \leq I_0 \leq 6$ in the ACORN catalogue reveal magnitudes that are higher than the values listed in the Austrian earthquake catalogue (Fig. 2a; ZAMG, 2020). The same is true for comparison of earthquakes recorded in the instrumental era 1906-2020 (Fig. 2b).

Comparison of the intensity-magnitude correlations in the ACORN catalogue for historical earthquakes ($M=0.6899I_0$) and instrumental earthquakes ($M=0.6864I_0$) reveals very little differences. Both correlations differ from intensity-magnitude correlations for historical earthquakes ($M=0.667I_0$) and instrumental earthquakes ($M=0.6549I_0$) used in the Austrian earthquake catalogue. (Fig. 2). Intensity-magnitude correlations in the Austrian catalogue therefore reveal systematically lower magnitude values for earthquakes, which were only recorded by their epicentral intensity. For intensity VII earthquakes the difference is about 0.2 magnitude scales. Nevertheless, we used the magnitudes provided in the catalogues for further calculations.

## 4. Complications, delustering and completeness analysis of the compiled catalogue covering the VBTFS

The recognition and removal of fore- and aftershocks from the raw catalogues is mandatory for further work based on the earthquake data such as the calculation of GR parameters and the assessment of catalogue completeness because it is generally assumed that earthquakes are poissonian-distributed and therefore independent of each other (Gardner and Knopoff, 1974; Shearer and Stark, 2011).

The earthquake data used in the current study were

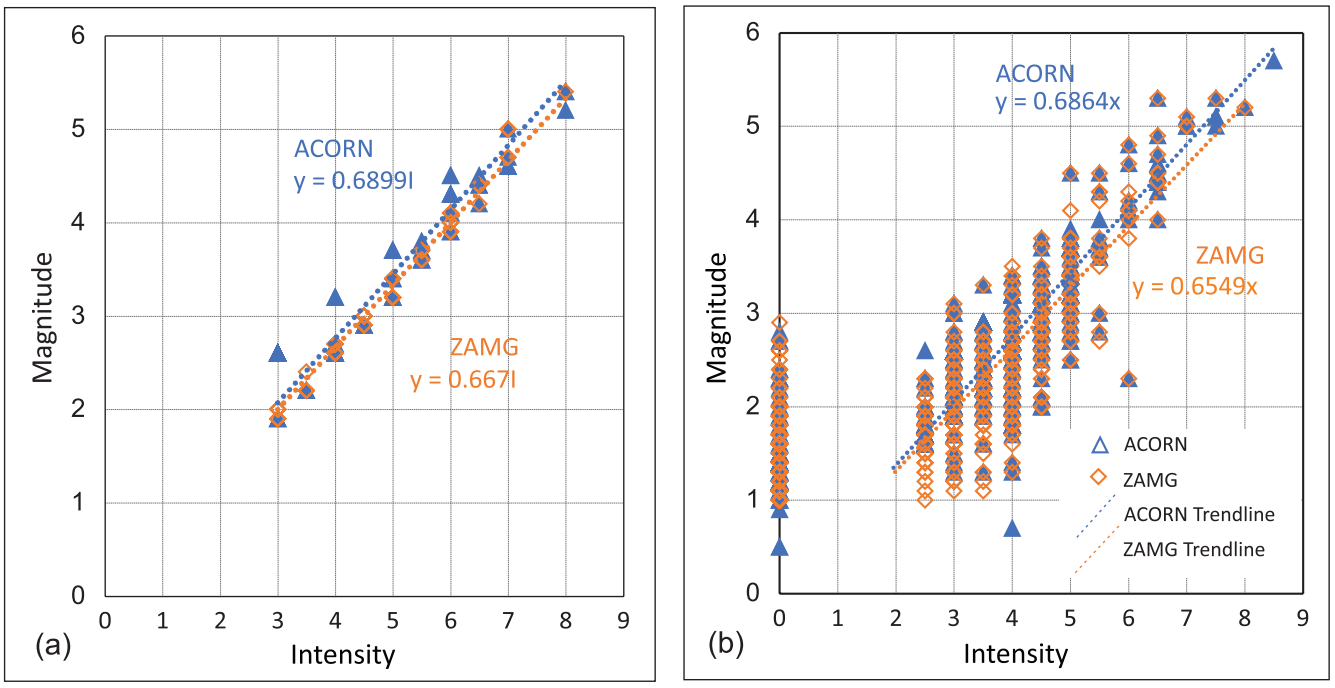


**Figure 2:** Intensity vs magnitude plot for earthquakes in the overlapping region of the ACORN (2004, blue triangles) and ZAMG (2020, orange diamonds) earthquake catalogues for historical earthquakes covering the time of 1267-1905 (a), and instrumental data covering the length of 1906-2020 (b). The ACORN earthquake catalogue stops in 2004.

compiled from the Austrian and ACORN earthquake catalogues to cover the whole extent of the VBTFS (Fig. 1). The compilation became necessary as existing regional catalogues such as the catalogue by Grünthal and Wahlström (2003) set the lower magnitude level for the catalogue entries at $M_w$=3.50. For the area of the VBTFS such a lower cut-off removes a large part of the recorded seismicity.

The seismic data for the VBTFS in ZAMG (2020) and ACORN (2004) comprises a magnitude range M=0.5-5.7 and cover a nominal time period of 754 years from 1267-2020 (738 years for the ACORN data). The clustered compiled earthquake catalogue records 1739 seismic events. Duplicate earthquakes have been removed manually for the area shown in Figure 1. For the overlap area the Austrian earthquake catalogue has been given priority and duplicate earthquakes were removed from the ACORN catalogue.

Figure 3 shows the distribution of earthquakes at VBTFS over time. The figure clearly shows that, although the nominal time coverage of the combined catalogue is about 750 years, only eight earthquake records are available from the period prior to 1800. Remarkable increases of the numbers of recorded earthquakes are observed around 1900 and close to the end of the 20$^{th}$ century.

Using the same method as in Nasir et al. (2013), the compiled data set was declustered manually using fault length-magnitude correlations to determine the maximum distance of aftershocks from the magnitude of the preceding mainshock (Wells and Coppersmith, 1994) and standard time windows after the mainshock according to Gardner and Knopoff (1974). To account for possible inaccurately determined earthquake locations the minimum distance is set to 10 km for the spatial window. For more detail we refer to Nasir et al. (2013; 2020). The earthquake data after declustering comprises 1603 earthquakes including 12 earthquakes with magnitudes greater than or equal to 5 (Fig. 3). Nine of these strong earthquakes were recorded in the last 135 years.

The compiled catalogue was subjected to completeness checks using two different methods. The reasons for repeating the completeness analyses reported by Nasir et al. (2013) are the use of an updated catalogue for Austria, which now extends up to 2020 and includes revisions made according to the historical earthquake research by Hammerl and Lenhardt (2013). Secondly, the region analyzed in this study is considerably larger than the area examined by Nasir et al. (2013), which did not extend to the Mur Mürz Fault.

### 4.1 TCEF completeness analysis

TCEF (Temporal Course of Earthquake Frequency) is the most widely used method for completeness analyses in Central Europe (e.g., Lenhardt, 1996; Grünthal et al., 1998). In this method, the cumulative number of earthquakes of a magnitude class is plotted versus time. Slope changes in the plot illustrate changes of the completeness of the catalogue (Nasir et al., 2013, Grünthal et al., 1998). It is common presumption that the latest steepening of the slope occurred when the data became complete for the magnitude class under consideration (Gasperini and Ferrari, 2000). Completeness-corrected recurrence intervals for each magnitude class are then calculated from the time interval corresponding to the latest linear segment of the curves and the number of records in this time interval (Nasir et al., 2013).

The overall analysis in Figure 4 shows significantly steepening slopes for all magnitude classes M<4 around 1900. These changes relate to the onset of regular earthquake records in the former Austro-Hungarian Empire in the aftermath of the 1895 Ljubljana earthquake. TCEF results further show that records of magnitude class 0≤M<1

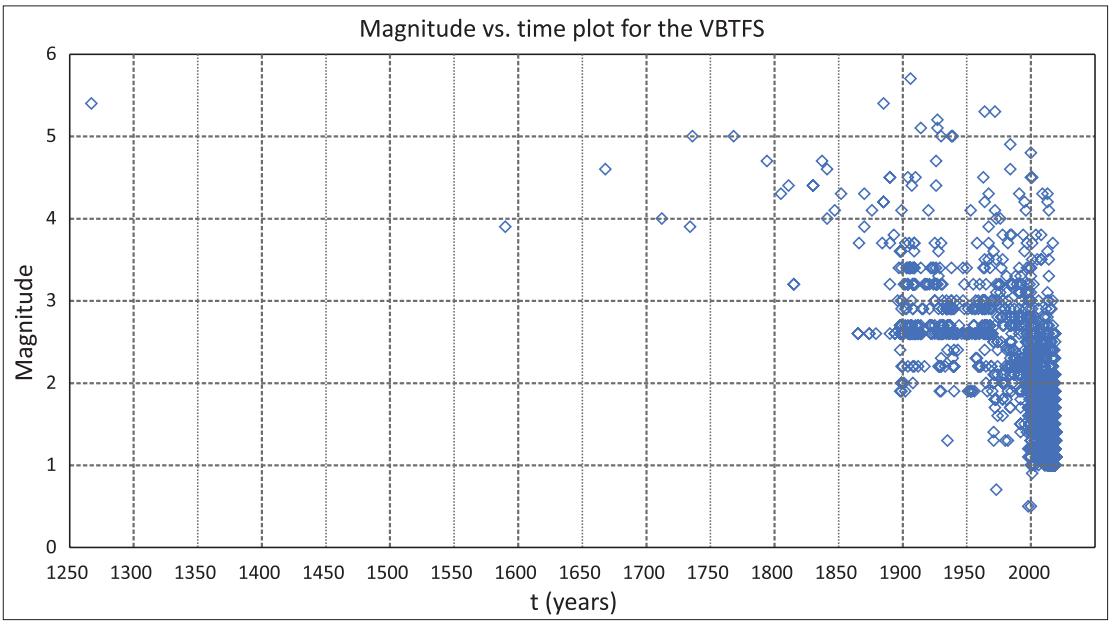


**Figure 3:** Magnitude vs. time plot from the combined catalogue (ZAMG, 2020; ACORN 2004).

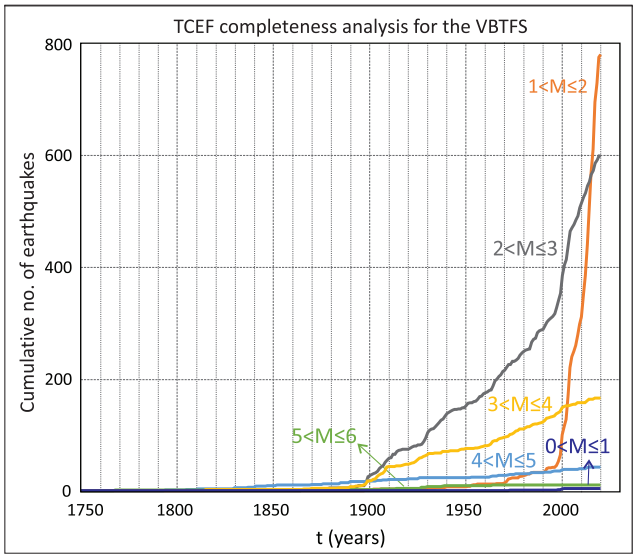


**Figure 4:** Cumulative number of earthquakes vs. time (TCEF) for the combined catalogue covering the VBTFS. The steepest slope in the plot for an individual magnitude class indicates that the catalogue is complete for that period of time. Note that the magnitude class 0≤M<1 never reaches completeness. Changes in slope for the intensity classes of 1≤M<2 and 2≤M<3 in 2004 are due to the ending of the ACORN catalogue in this year.

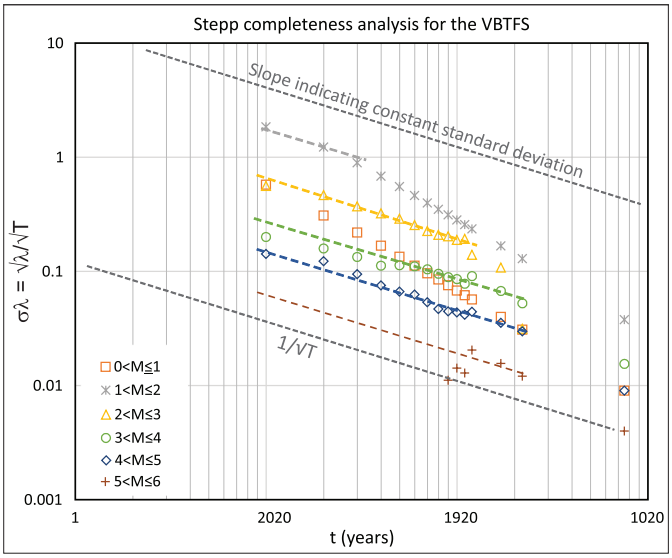


**Figure 5:** Stepp completeness analysis of the combined catalogue covering the VBTFS. The graph shows the standard deviation of mean rate of earthquakes occurrences plotted vs. time. Colours indicate individual magnitude classes. The catalogue is regarded complete for the time period for which the standard deviation (σ) of the mean recurrence rate (λ) of earthquakes of a given magnitude class follows the dashed 1/√T trend line. Where it deviates from that line, the catalogue is considered incomplete. Note that the magnitude class of 0≤M<1 never reached completeness.

cannot be regarded complete at any time because the slope of the corresponding curve is much lower than the one of intensity class 1≤M<2 indicating that by far not all events with M<1 were recorded in recent years. Periods of complete records along the VBTFS range from 24 years for magnitude class 1≤M<2 to 223 years for magnitude class 4≤M<5. For magnitude class 5≤M<6, which contains only 12 earthquakes, complete records are estimated to start in 1884 (Table 1).

### 4.2 Stepp completeness analysis

Stepp (1972) proposed a statistical approach to analyze catalogue completeness. The test relies on the statistical property of the Poisson distribution highlighting time intervals during which the recorded earthquake occurrence rate is uniform (Stepp, 1972). The method was described in detail by Nasir et al. (2013). The magnitude classes are analyzed for completeness using time windows of different length in the time period between 1267 and 2020 (754 years; Fig. 5). The calculation uses ten time windows of 10 years (1901-2020), two time windows of 50 years (1801-1900) and one time-window covering 534 years (1267-1800). The corresponding completeness of all magnitude classes are estimated manually from the parts of the calculated curves that follow a linear trend parallel to $1/\sqrt{T}$ line. For the corresponding time intervals, the mean rate of occurrence of earthquakes of the analyzed magnitude class is stable.

The completeness period for 1≤M<2 is 20 years (2001-2020), for 2≤M<3 110 years (1911-2020), for 3 ≤ M < 4 and 4 ≤ M < 5 220 years (1801-2020). For the highest magnitude class 5 ≤ M < 6, the catalogue is regarded complete since 1875. The intensity-based completeness analysis for VBTFS (Nasir et al., 2013) in comparison revealed 109 years to 209 years completeness time windows for the intensity classes III<$I_0$≤IV and VI<$I_0$≤VII. Intensity class VII<$I_0$≤VIII did not include enough earthquakes to calculate a stable recurrence interval.

| M | Completeness period (TCEF) |
|---|---|
| 1<M≤2 | 1997-2020 |
| 2<M≤3 | 1997-2020 |
| 3<M≤4 | 1885-2020 |
| 4<M≤5 | 1830-2020 |
| 5<M≤6 | 1885-2020 |

**Table 1:** TCEF derived periods of complete earthquake records along the VBTFS.

| Magnitude | Completeness period (Stepp Test) |
|---|---|
| 1<M≤2 | 2001-2020 |
| 2<M≤3 | 1911-2020 |
| 3<M≤4 | 1801-2020 |
| 4<M≤5 | 1801-2020 |
| 5<M≤6 | 1875-2020 |

**Table 2:** Periods of complete earthquake records derived from the Stepp test (Stepp, 1972).

## 5. Long and short-duration aftershock sequences

Large earthquakes are typically followed by aftershock activity, which generally is assumed to decay hyperbolically as stated by Omori's law (Ogata, 1983). Based on empirical data, Stein and Liu (2009), on the other hand, suggested that large earthquakes may have much longer aftershock sequences, which depend on the slip rate of faults and may last for decades or even centuries. At the VBTFS, the seismicity following the 1906 Dobrá Voda earthquake was identified as an example of such a long aftershock sequence (Nasir et al., 2020). Deciding whether the earthquake activity in a defined region can be related to a long aftershock activity subsequent to a strong earthquake is challenging because the definition of aftershock activity depends on numerous parameters such as the definition of the area treated as aftershock zone and the level of background seismicity before the mainshock (Stein and Liu, 2009).

Figure 6 illustrates two examples of short- and long-term patterns of decaying earthquake activity forming aftershock sequences. Seismicity subsequent to the 1906 Dobrá Voda earthquake (Fig. 6a) was described in detail by Nasir et al. (2020). The Dobrá Voda earthquake of 09.01.1906 (M=5.7) at the VBTFS in Slovakia initiated earthquake activity in vicinity of the mainshock (< 13 km) which is gradually decaying since 1906. The pattern shown in Figure 6a suggests that aftershock activity extends to the present. Figure 6b, on the other hand, shows the seismicity in the time before and after the 11.07.2000 (M=4.8) Ebreichsdorf earthquake. In this case the aftershock activity decayed hyperbolically and reached the level of background seismicity within about 300 days after the mainshock.

In order to identify seismicity patterns that may be indicative of long-term aftershock sequences comparable to the 1906 Dobrá Voda example, we divide the VBTFS into arbitrarily selected segments. Seismicity recorded within each of these segments is further analyzed to check whether it shows distinctive patterns of decaying earthquake activity which may be related to long aftershock sequences. The purpose is to identify possible strong earthquakes which occurred before the start of records in the earthquake catalogue, and which may become "visible" due to their aftershock sequences.

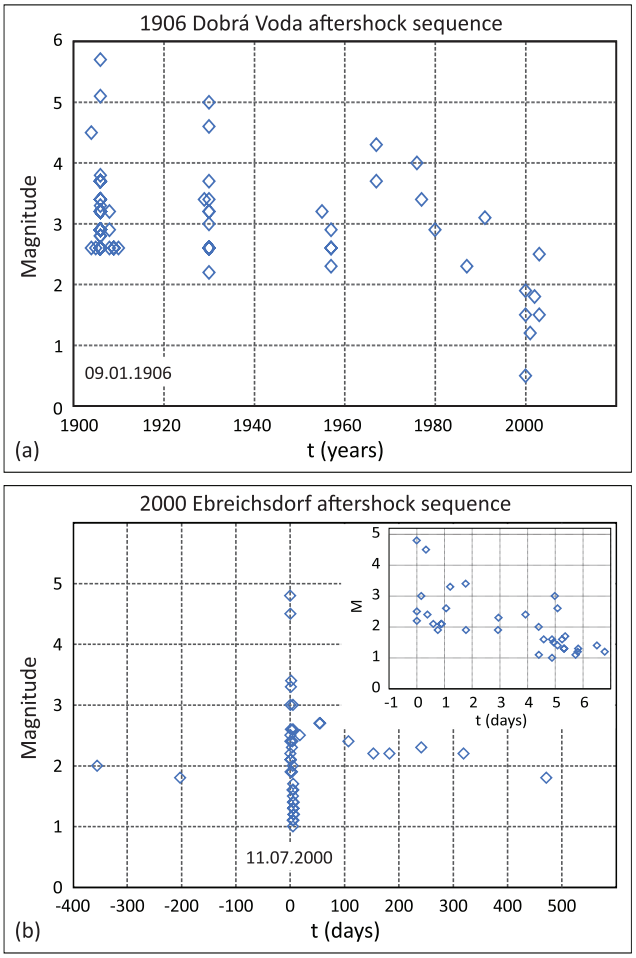


**Figure 6:** Different pattern of decaying earthquake activity. (a) Long aftershock sequence of 09.01.1906 (M=5.7) Dobrá Voda earthquake. Note that time is provided in years. (b) Short (Omori-type) aftershock sequence subsequent to the 11.07.2000 (M=4.8) Ebreichsdorf earthquake. The inset in Fig 6(b) shows aftershocks in the first 7 days after the mainshock.

## 6. Seismicity of arbitrarily selected segments of the VBTFS

The VBTFS is divided into eight segments of approximately 50 km length. Segments are selected to overlap each other for not missing possible aftershock sequences which followed earthquakes that occurred close to one of the segment boundaries (Fig. 7). The arbitrarily selected segment boundaries do not agree with the kinematic fault segments of the VBTFS defined based on fault geometry (Hinsch and Decker, 2011; Beidinger and Decker, 2011). The selection of segment lengths of about 50 km is driven by the MCE estimates of M=6.0-6.8 for the VBTFS (Decker and Hintersberger, 2011). Earthquakes with such

| Segment no. | GR a- and b-values calculated for: | | | |
|---|---|---|---|---|
| | Total catalogue length | | Completeness period | |
| | a | b | a | b |
| 1 | 2.08 | 0.68 | 2.31 | 0.67 |
| 2 | 1.05 | 0.50 | 1.20 | 0.49 |
| 3 | - | - | 1.34 | 0.49 |
| 4 | 1.48 | 0.63 | 1.99 | 0.66 |
| 5 | 1.86 | 0.70 | 2.43 | 0.76 |
| 6 | 1.47 | 0.63 | 2.39 | 0.69 |
| 7 | 1.06 | 0.60 | 2.12 | 0.71 |
| 8 | 0.81 | 0.47 | 2.54 | 0.86 |

**Table 3:** a- and b-values of the Gutenberg-Richter relations calculated for eight segments of the VBTFS. See Figure 8 for segment location. In segment 3 the total catalogue length is equal to the completeness period (earthquake records start in 1890).

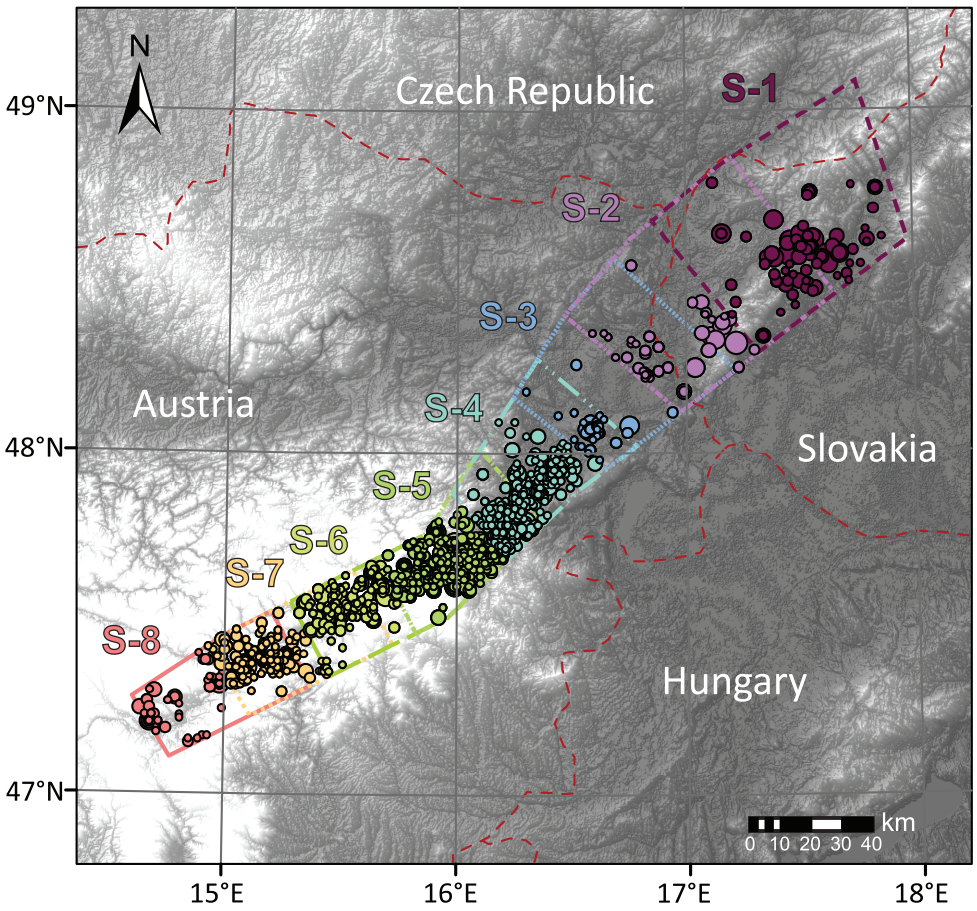


**Figure 7:** Subdivision of the VBTFS into 8 arbitrary overlapping segments of about 50 km length (S-1 to S-8) used for the analysis of aftershock sequences and calculation of GR-parameters. See text for further explanation.

magnitudes are broadly associated with slip on <50 km long faults (Wells and Coppersmith, 1994). It is therefore assumed that for each possible strong earthquake the full length of the slipped fault is contained by one of the segments. The selection of segment length and overlaps is further guided by the consideration of inaccuracies of epicenter locations of historical earthquake data and the necessity of a minimum number of earthquakes for defining GR relations.

Segments 1 and 2 are located in Slovakia and include the strongest earthquake recorded at the VBTFS (1906 Dobrá Voda, M=5.7). The segments contain 207 and 96 earthquakes with M=0.5-5.7, respectively. Time coverage is 1805-2004 (segment 1) and 1794-2017 (segment 2). The first data entries in segment 1 (1805, M=4.3) and segment 2 (1794, M= 2.6) are followed by a data gap until 1852 (M=4.3). Time series of both overlapping segments 1 and 2 show a general decay of seismicity, which starts with the 1906 Dobrá Voda (M=5.7) earthquake (Fig. 8). The temporal evolution of seismicity in segment 1 around Dobrá Voda reveals a level of background seismicity with M=2.6-4.3 (11 earthquakes) recorded between about 1800 and 1906. While the significant earthquakes (M=4-5) in the time before 1906 are scattered over the entire region, seismicity concentrates within a distance of less than 13 km from the epicenter after the 1906 Dobrá Voda mainshock, (Nasir et al., 2020). The time-magnitude plot includes a second strong earthquake in 1914 (M=5.1) which is regarded as an aftershock of the 1906 event. The distance between the epicenters of the two events is 33 km. The slow regular decrease of the largest observed magnitudes over time until 2004 (end of the ACORN catalogue) suggests that the aftershock sequence lasted much longer than predicted by the Omori law. The level of background seismicity with M=2.6-4.3 (11 earthquakes) recorded before the 1906 Dobrá Voda earthquake between about 1800 and 1900 is only reached about 100 years after the mainshock.

Segment 3 covers the border region between Austria and Slovakia. It includes 78 earthquakes with M=1-5.2 for the time period 1890 to 2017 (Fig. 8). The time plot shows 4 earthquakes in 1890 including a mainshock (M=4.5) and three aftershocks with different epicenter locations within distances of 5 km from mainshock (Fig. 8). The 1927 Schwadorf earthquake (M=5.2) is followed by a short aftershock sequence. The apparent long-term decay of seismicity in the temporal window cannot be regarded to be related to aftershock activity due to the distance of events from the Schwadorf mainshock (Fig. 8).

Magnitudes recorded in segment 4 range from M=1-5.2 with data length from 1590-2019 and a total number of 487 earthquakes (Fig. 8). This segment shows no tem-

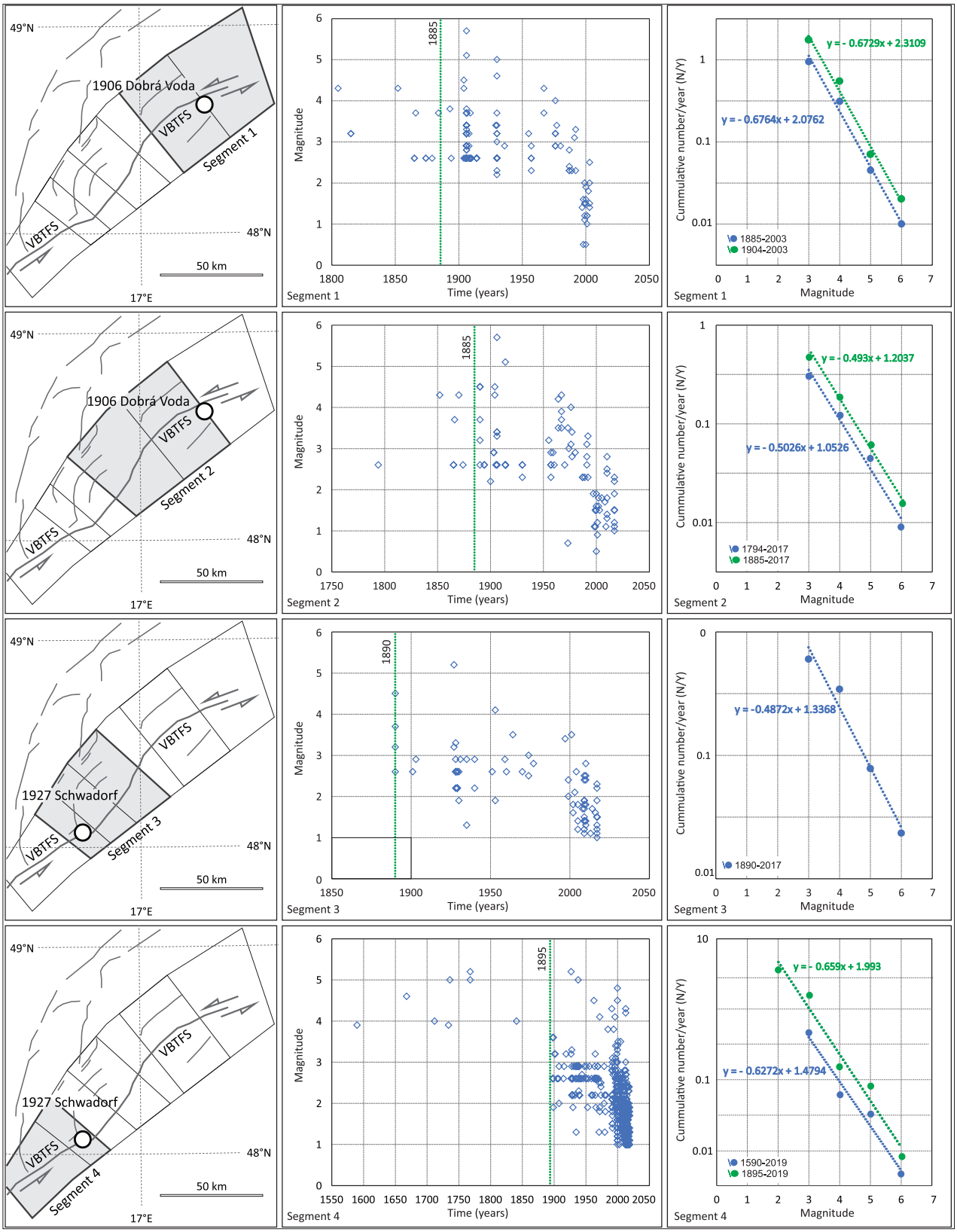


**Figure 8:** Left column: Location of segments 1-8. Center: time vs. magnitude plots. Green line shows the visually estimated start of catalogue completeness with respect to earthquakes with M≥3. Right column: Gutenberg-Richter diagrams for segments 1-8 of the VBTFS.

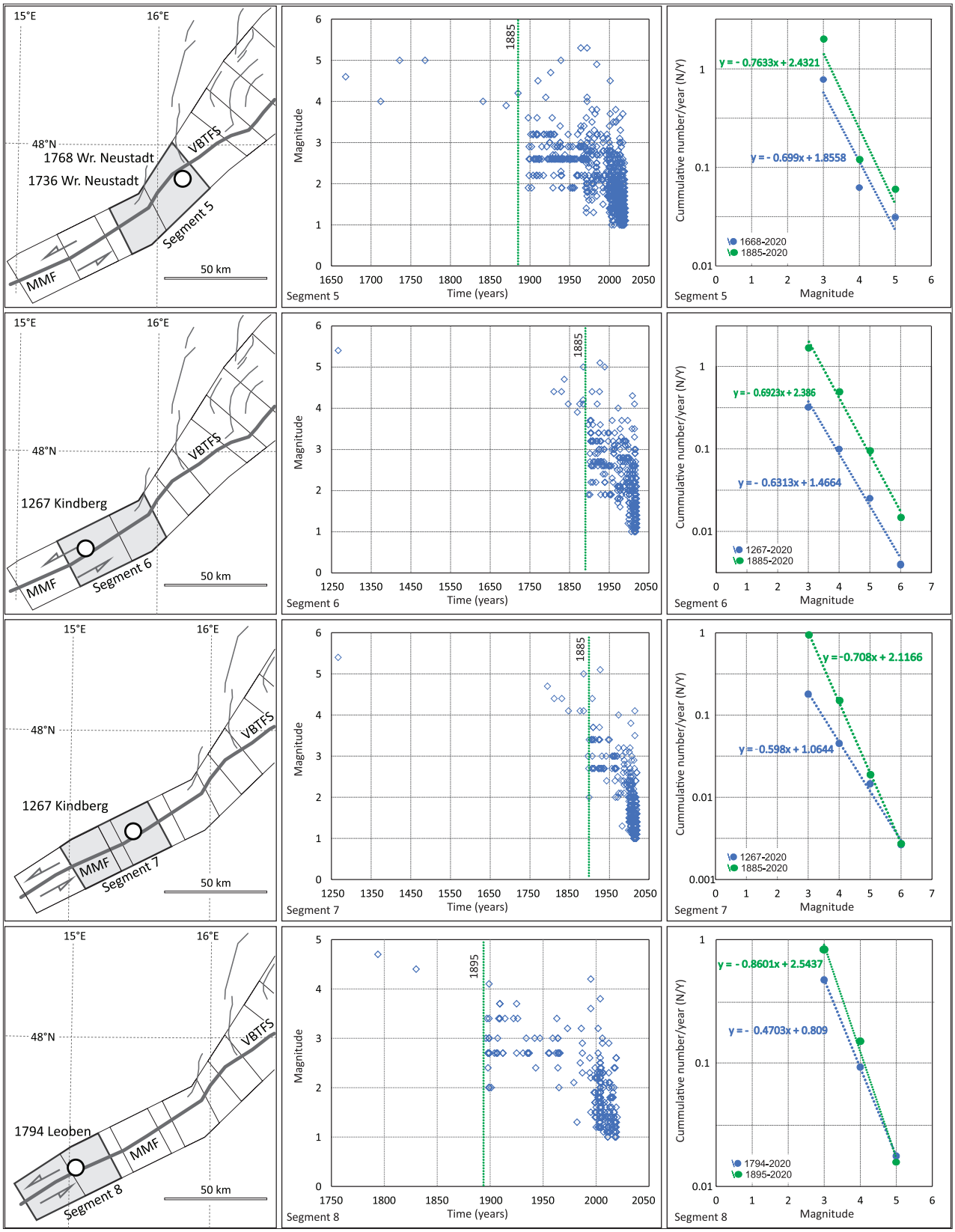


**Figure 8:** Continued.

poral seismicity pattern that could indicate gradual decays of seismicity except for the 1927 Schwadorf (M=5.2) earthquake (see above).

For segment 5 magnitudes between M=1-5.3 were recorded for 673 events between 1668 and 2020. Records start from 1668 with M=4.6 at Wiener Neustadt (ACORN, 2004) followed by another earthquake in 1712 having M=4 at the same epicenter (Fig. 8). It must be noted that the 1668 event has been excluded from ZAMG (2020) based on the assessment by Hammerl and Lenhardt (2013). The next M=5 earthquake occurred at a distance of 5 km from Wiener Neustadt (Neudörfl) in 1736. For the next stronger event on 1768 (M=5) ZAMG (2020) also lists an epicenter at about 5 km distance from Wiener Neustadt. In sum, 5 out of 7 earthquakes recorded between 1668 and 1841 are listed with epicenters in close proximity to each other. It can, however, not be judged if the observed clustering correctly reflects the spatial distribution of seismicity, or it is due to inaccurate location of the historical events (compare Gangl and Decker, 2011). In the time before 1898 only 7 earthquakes were recorded in a period of 230 years. Seismicity patterns indicative of aftershock sequences are not evident. Distances between the epicenters of earthquakes between 1898 and 1964 that might indicate an apparent increase of the maximum recorded magnitudes from about M=4 to M=5.3 are too large to identify the events as fore- or aftershocks.

Segment 6 includes 506 earthquakes with M=1-5.4 that occurred between 1267 and 2020. The significant recorded earthquakes are 1267 Kindberg (M=5.4), 1811 Krieglach (M=4.4), 1830 Mürzzuschlag (M=4.4) and 1837 Mürzzuschlag (M=4.7; Fig. 8). The magnitude-time plot does not include any pattern indicative of aftershocks. All earthquakes are randomly distributed over the approximately 50 km long segment.

The nominal record length for segment 7 covers 754 years (362 earthquakes). Records, however, contain no data for the 527 years between 1267 (Kindberg, M=5.4) and 1794 (Leoben, M=4.7). The next notable earthquakes followed in 1811 (Krieglach, M=4.4), 1830 (Leoben, M=4.4) and 1847 (Kindberg, M=4.1). ZAMG (2020) places the earthquakes in 1794 and 1830 within 1.3 km distance (Leoben). The other three events mentioned above occurred at distances of 10km from each other. The distance of 40 km between the two groups, however, does not suggest linkage.

For segment 8, ZAMG (2020) lists 259 earthquakes with the first data entry of the 1794 Leoben earthquake. From the time between 1794 and 1899 only two earthquakes are secured by historical records. In spite of the poor data coverage, the time-magnitude plot shows a gradual decrease of the largest observed magnitudes between 1794 and the 1980ies. The strongest events of this row (1794 Leoben; 1830 Leoben; 1899 St. Stefan) occurred at a nominal distance of some 10 km not contradicting an interpretation as aftershocks. Interpreting the declining seismicity as a long aftershock sequence of a strong earthquake must, however, remain uncertain because of the poor earthquake record and the inaccuracies inherent in the determination of the historical epicenters.

The GR-trendlines consider data from the time window between the first recorded earthquake at the segment and 2020 (blue) and the period for which the record of $M \geq 3$ events is estimated to be complete as indicated in the corresponding time-magnitude plots (green), respectively. Segment 1 and the overlapping segment 2 show the 1906 Dobrá Voda long aftershock sequence. The time-magnitude diagram for segment 3 shows decaying seismicity after the 1927 Schwadorf earthquake. Segment 4 is including the short aftershock sequence following the 2000 Ebreichsdorf mainshock (compare Fig. 6b). Note that segments 3 to 7 do not show temporal seismicity patterns comparable to the long-term decay after the 1906 Dobrá Voda earthquake (segment 1 and 2). Segment 8 shows a regular decrease of the largest recorded magnitudes after the 1794 Leoben earthquake that is comparable to the patterns subsequent to 1906 Dobrá Voda and might indicate a long aftershock sequence.

In addition to the temporal distribution of seismicity along the VBTFS, we analyzed the frequency-magnitude correlation of earthquakes for the whole fault system and the 8 selected fault segments. The correlation is stated by the GR relation which can be written as

$$\log N(Mc) = a - bM$$

where N is the number of events with magnitudes larger than the magnitude of completeness Mc and a is the corresponding level of seismic activity (Gutenberg and Richter, 1942).

Figure 9 shows the results of calculating GR relations

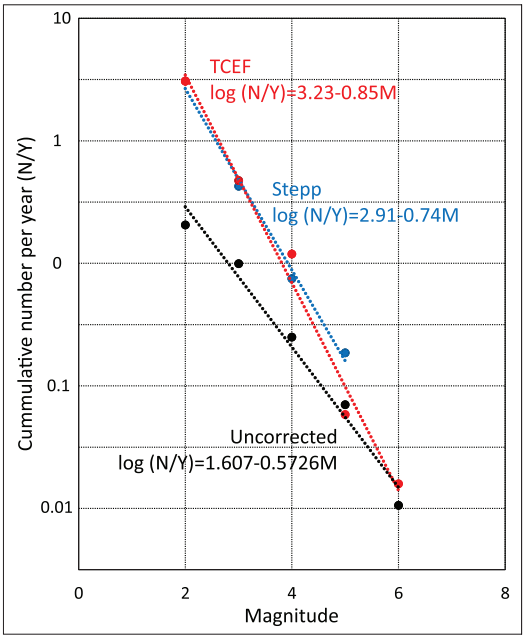


**Figure 9:** Comparison of Gutenberg-Richter relations obtained for the VBTFS from the declustered compiled catalogue without applying completeness correction (black), after TCEF completeness correction (red) and after Stepp correction (blue). See text for discussion.

for the entire VBTFS. The graph shows that the actual values of the GR a- and b-values differ when using different completeness corrections. Without applying any correction, the b-value obtained from the declustered catalogue of the VBTFS is 0.57 which is low for a seismically active region. Applying the Stepp and TCEF corrections leads to a significant increase of the a-values. The b-values after TCEF and Stepp correction are 0.85 and 0.74 (Fig. 9). The b-value calculated for the VBTFS from the catalogue without completeness correction leads to underestimate the number of earthquakes with smaller and medium magnitudes. The frequencies of small magnitude earthquakes resulting from TCEF and Stepp correction is almost identical. The TCEF correction, however, seems to underestimate the frequency of earthquakes of higher magnitudes by the higher b-value because TCEF includes the highest magnitude earthquakes based on the assumption that records of these earthquakes are complete for the whole length of the catalogue. Stepp completeness analysis, however, shows that the number of earthquakes of the highest magnitude class ($5<M\leq6$) is too small to calculate a reliable recurrence rate. The corresponding data is therefore not considered in the GR calculation (see Nasir et al., 2013, for a more detailed discussion). We regard the results obtained after Stepp correction to be more reliable for extrapolating the recurrence periods of large magnitude earthquakes.

The GR relations calculated for the 8 arbitrarily selected segments of the VBTFS are shown in Figure 8. The GR values were calculated from the uncorrected clustered catalogue as it was not possible to apply completeness correction on individual segments. The numbers of recorded earthquakes in the individual segments proved insufficient for applying the TCEF or Stepp method for each magnitude class. To assess the resulting errors, we calculate GR-values of all segments for two time periods: (a) the nominal time coverage of the catalogues for each segment starting from the oldest recorded earthquake; and (b) the time period for which visual inspection of the time-magnitude graphs in Fig. 8 suggest completeness for $M\geq3$ earthquakes, i.e., starting from 1885 or 1895. These estimated completeness periods are corroborated by the TCEF and Stepp analyses (Tab. 1,2).

Comparison of the GR values obtained for the different time windows shows that a- and b-values are calculated from the nominal time coverage of the catalogue are systematically smaller than the values obtained from the time window corresponding to the assumed complete records. This is due to the widely incomplete record of small and medium earthquakes before about 1885. The

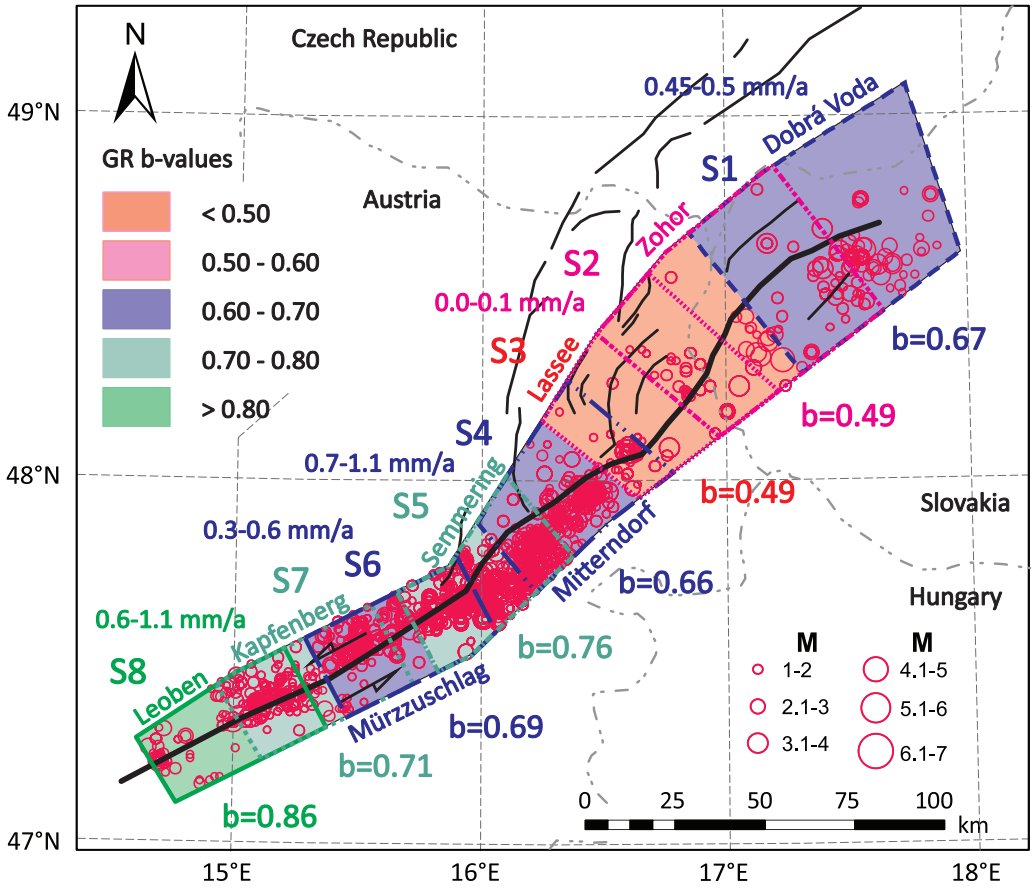


**Figure 10:** Gutenberg-Richter b-values calculated for eight arbitrarily selected overlapping fault segments and the time period for which time-magnitude graphs in Fig. 8 suggest completeness for $M\geq3$ earthquakes. Note the variation of b-values ranging from 0.49 to 0.86. Fault segments with low levels of historical and instrumental seismicity and low seismic slip rates (S2 and S3) are characterized by low GR b-values. Seismic slip rates from Hinsch and Decker (2011).

results further show that both, GR a- and b-values vary significantly between the segments. For the assumed completeness period since about 1885 a-values reach from 1.20 to 2.54 and b-values from 0.49 to 0.86 (b-values; Fig. 10). The smallest b-values (0.49) are calculated for segments 2 and 3. Visual inspection of the seismicity along the VBTFS shows that these segments are characterized by the lowest earthquake activity in historical times (Fig. 10).

## 7. Discussion and conclusions

The analysis of time sequences of earthquakes recorded in 8 arbitrarily selected segments of the VBTFS was performed to identify possible long aftershock sequences subsequent to major earthquakes. The analyses were stimulated by Stein and Liu (2009) who suggest aftershock durations of tens to several hundreds of years for slow moving faults with fault loading rates of few mm/year. Nasir et al. (2020) show that this model is at least applicable to the 1906 Dobrá Voda (M=5.7) earthquake, which is followed by a century-long aftershock sequence.

Assessments of earthquake time sequences along the VBTFS is strongly limited by the length and the completeness of available earthquake records. TCEF and Stepp completeness tests show that tolerably complete records only exist for the last about 200-300 years.

With exception of segment 8, time sequences obtained for fault segments apart from the 1906 Dobrá Voda (M=5.7) earthquake did not reveal long-term decays of seismicity that might be interpreted as long aftershock sequences. Segment 8, covering the southwestern tip of the VBTFS, revealed a 200 years long gradual decrease of the largest observed magnitudes starting with the 1794 Leoben (M=4.7) earthquake. Epicentral distances of the largest events in the row allow an interpretation as aftershocks. The 1794 event is the oldest earthquake listed in the catalogue for the region under consideration. It must therefore remain open if the recorded decay of seismicity results from the 1794 event, or a still older, possibly stronger earthquake before. The latter is corroborated by the low magnitude of the 1794 earthquake which would typically not be considered to cause long aftershock sequences. The 2000 Ebreichsdorf (M=4.8) earthquake, contained in segment 4, was followed by an Omori-type aftershock sequence which lasted for a few hundred days only.

Calculations of the GR relations for the 8 analyzed fault segments reveal differences between the a- and b-values of the individual segments (Figs 8, 10). Segments 2 and 3 with the lowest b-values of 0.49 coincide with those parts of the VBTFS for which Hinsch and Decker (2011) calculated the largest seismic slip deficits by comparing the seismic energy release and geodetically/geologically derived slip rates of the VBTFS. For the part of the VBTFS in segment 3 of this study Hinsch and Decker (2011) state seismic slip rates between 0 and 0.1 mm/a. These rates are much lower than geodetically/geologically derived slip velocities in the range of 1-2 mm/a. The high b-values of 0.67 and 0.76 are calculated for segments 1 and 5 which, on the other hand, include parts of the VBTFS with seismic slip rates of about 0.5 mm/a (Dobrá Voda area) and 0.7-1.1 mm/a (northeastern part of the Mur-Mürz fault and southwestern Vienna Basin). Data therefore indicate that GR b-values correlate negatively with the seismic slip deficit of the VBTFS. A similar negative correlation of b-values and the slip deficit rate was reported by Nanjo and Yoshida (2018).

Variations of the GR b-value are commonly related to different states of stress in the deformation zone (Scholz, 1968; 2015) with low b-values indicating high differential stress (Farrell et al., 2009; Scholz, 2015). GR b-values are therefore considered to be proxies of stress which identify highly stressed fault segments or asperities that resist slip (Schorlemmer and Wiemer 2005; Nuannin, 2006). Low b-values were also related to knickpoints and changes of fault strike (Öncel et al., 1996). It is assumed that such highly stressed segments are locations where future ruptures are likely to occur (Schorlemmer and Wiemer, 2005; Bayrak and Bayrak, 2012; Hussain et al., 2020). At least for plate boundaries, this assumption is corroborated by the finding that small b-values characterized the focal areas of strong earthquakes prior to fault rupture (Nanjo et al., 2012; Nanjo and Yoshida, 2021).

For the VBTFS, fault segments with high seismic slip deficits such as the ones next to the Lassee- and Zohor segments (see Fig. 10 for location) were previously interpreted as "locked" fault segments which have a significant potential to release future strong earthquakes, in spite of the fact that historical and instrumentally recorded seismicity is very low (Hinsch and Decker, 2003; 2011). This interpretation is corroborated by the low b-values that suggest high differential stresses for these segments.

## Acknowledgements

We thank Seth Stein for his stimulating discussion on aftershock sequences during the Fragile Earth conference in Munich. We gratefully acknowledge the careful and very constructive reviews by Ewald Brückl and Christoph von Hagke. Their comments and suggestions helped improving the manuscript considerably.

## References

ACORN, 2004. Catalogue of Earthquakes in the Region of the Alps - Western Carpathians– Bohemian Massif for the period from 1267 to 2004. Computer File, Vienna (Central Institute for Meteorology and Geodynamics, Department of Geophysics). Brno (Institute of Physics of the Earth, University Brno.

Bayrak Y., Bayrak E., 2012. Regional variations and correlations of Gutenberg–Richter parameters and fractal dimension for the different seismogenic zones in Western Anatolia. Journal of Asian Earth Sciences, 58, 98–107.

Beidinger A., Decker K., 2011. 3D geometry and kinematics of the Lassee flower structure: Implications for segmentation and seismotectonics of the Vienna Basin strike–slip fault, Austria. Tectonophysics, 499, 22-40. doi: 10.1016/j.tecto.2010.11.006

Brückl E., Behm M., Decker K., Grad M., Guterch A., Keller R., Thybo H., 2010. Crustal structure and active tectonics in the Eastern Alps. Tectonics 29, 279–295.

Decker K., 1996. Miocene tectonics at the Alpine–Carpathian junction and the evolution of the Vienna Basin. Mitteilungen der Gesellschaft der Geologie- und Bergbaustudenten, 41, 33–44.

Decker K., Hintersberger E., 2011. Assessing Maximum Credible Earthquake (MCE) Magnitudes for a Slow Intra-Plate fault system in the Vienna Basin, Austria. Seismological Research Letters, 82/2, 300.

Decker K., Peresson H., 1996. Tertiary kinematics in the Alpine-Carpathian-Pannonian system: links between thrusting, transform faulting and crustal extension, In: Wessely G., Liebl W. (Editors), Oil and Gas in Alpidic Thrustbelts and Basins of Central and Eastern Europe, European Association of Geoscientists and Engineers, 5, 69-77.

Decker K., Persson H., Hinsch R., 2005. Active tectonics and Quaternary basin formation along the Vienna Basin Transform fault. Quaternary Science Reviews, 24,307-322.

Farrell J., Husen S., Smith R.B., 2009. Earthquake swarm and b-value characterization of the Yellowstone volcano-tectonic system. Journal of Volcanology and Geothermal Research, 188, 260-276.

Gangl G., Decker K., 2011. Österreichische Starkbeben mit Intensität ab Grad 7. Österreichische Ingenieur- und Architekten-Zeitschrift, 156, 229-237.

Gardner J.K., Knopoff L., 1974. Is the sequence of earthquakes in southern California, with aftershocks removed, poissonian? Bulletin of the seismological Society of America, 64, 1363-136

Gasperini P., Ferrari G., 2000. Deriving numerical estimates from descriptive information: the computation of earthquake parameters. In Catalogue of Strong Italian Earthquakes from 461 B.C. to 1997. Annali di Geofisica, 43/4, 729-746.

Grenerczy G., Kenyeres A., Fejes I., 2000. Present crustal movement and strain distribution in Central Europe inferred from GPS measurements. Journal of Geophysical Research, 105/B9, 21835-21846.

Grenerczy G., Sella G., Stein S., Kenyeres A., 2005 Tectonic implications of the GPS velocity field in the northern Adriatic region. Geophysical Research Letters, 32, L16311, doi:10.1029/2005GL022947

Grünthal G., Mayer-Rosa D., Lenhardt W., 1998. Abschätzung der Erdbebengefährdung für die D-A-CH-Staaten - Deutschland, Österreich, Schweiz. Bautechnik, 75/10, 753-767.

Grünthal G., Wahlström R., 2003. An $M_w$ based earthquake catalogue for central, northern and northwestern Europe using a hierarchy of magnitude conversions. Journal of seismology, 7/4, 507-531.

Grünthal G., Wahlström R., Stromeyer D., 2009. The unified catalogue of earthquakes in central, northern, and northwestern Europe (CENEC)—updated and expanded to the last millennium. Journal of Seismology, 13, 517-541. doi:10.1007/s10950-008-9144-9

Gutdeutsch R., Aric K., 1988. Seismicity and neotectonics of the East Alpine–Carpathian and Pannonian area. American Association Petroleum Geologists, Memoir 45, 183-194.

Gutenberg B., Richter C.F., 1942. Earthquake magnitude, intensity, energy and acceleration. Bulletin of the Seimological Society of America, 32, 163-191.

Hainzl S., Zöller G., Scherbaum F., 2003. Earthquake clusters resulting from delayed rupture propagation in finite fault segments. Journal of Geophysical Research, 108,/B1. doi:10.1029/2001JB000610

Hammerl C., Lenhardt W., 2013. Erdbeben in Niederösterreich von 1000 bis 2009 n. Chr. Abhandlungen der Geologischen Bundesanstalt, 67, 3-297.

Hinsch R., Decker K., 2003. Do seismic slip deficits indicate an underestimated earthquake potential along the Vienna Basin Transform Fault System? Terra Nova, 15/5, 343-349.

Hinsch R., Decker K., 2011. Seismic slip rates, potential subsurface rupture areas and seismic potential of the Vienna Basin Transfer Fault. International Journal of Earth Science, 100, 1925-1935. doi: 10.1007/s00531-010-0613-3

Hintersberger E., Decker K., Lüthgens C., Fiebieg M., 2014. Geological evidence for earthquakes close to the destroyed Roman city of Carnuntum. Schriftenreihe der der Deutschen Gesellschaft für Geowissenschaften, 85, 443.

Hussain H., Shuangxi Z., Usman M., Abid M., 2020. Spatial variation of b-values and their relationship with the fault blocks in the western part of the Tibetan Plateau and its surrounding area. Entropy, MDPI, 22, 1016. https://doi.org/10.3390/e22091016

Kröll A., Wessely G., 1993. Wiener Becken und angrenzende Gebiete - Strukturkarte-Basis der tertiären Beckenfüllung. Geologische Themenkarte der Republik Österreich 1:200.000, Geologische Bundesanstalt, Wien.

Lenhardt W., 1996. Erdbebenkennwerte zur Berechnung der Talsperren Österreichs. Bundesministerium für Land- und Forstwirtschaft. Österreichische Staubeckenkommission, Wien 1996, 85 pp.

Lenhardt W., Freudenthaler C., Lippitsch R., Fiegeil E., 2007a. Focal depth distribution in the Austrian Eastern Alps based on macroseismic data. Austrian Journal of Earth Sciences, 100, 66-79.

Lenhardt W., Svancara J., Melichar P., Pazdirkova J., Havir J., Sykorova Y., 2007b. Seismic activity of the Alpine-Carpathian-Bohemian massif region with regard to geological and potential field data. Geologica Carpathica, 58, 397-412.

Linzer H. G., Decker K., Peresson H., Dell'Mour R., Frisch W. 2002. Balancing lateral orogenic float of the Eastern Alps. Tectonophysics, 354/3-4, 211-237.

Möller G., Brückl E., Weber R., 2011. Active tectonic deformation at the transition from the European and Pannonian domain monitored by a local GNSS network. Vermessung & Geoinformation, 2/2011: 138-148.

Nanjo K.Z., Hirata N., Obara K., Kasahara K., 2012. Decade-scale decrease in b value prior to the M9-class 2011 Tohoku and 2004 Sumatra quakes. Geophysical Research Letters, 39, L20304, doi:10.1029/2012GL052997.

Nanjo K.Z., Yoshida A., 2018. A b map implying the first eastern rupture of the Nankai Trough earthquakes. Nature communications, 9/1, 1-7. DOI: 10.1038/s41467-018-03514-3

Nanjo K.Z., Yoshida A., 2021. A b map implying the first eastern rupture of the Nankai Trough earthquakes. Nature Communications, 9: 1117, DOI: 10.1038/s41467-018-03514-3

Nasir A., Hintersberger E., Decker K., 2020. The 1906 Dobrá Voda Earthquake (M=5.7) at the Vienna Basin Transfer Fault: evaluation of the ESI2007 intensity and analysis of the aftershock sequence. Austrian Journal of Earth Sciences, 113/1, 43-58. doi:10.17738/ajes.2020.0003.

Nasir A., Lenhardt W., Hintersberger E., Decker K., 2013. Assessing the completeness of historical earthquake and instrumental data in Austria and the surrounding areas. Austrian Journal of Earth Sciences, 106/1, 90-102.

Nuannin P., 2006. The Potential of b-value Variations as Earthquake Precursors for Small and Large Events. Digital Comprehensive Summaries of Uppsala Dissertations from the Faculty of Science and Technology 183, Uppsala Universitet, ISBN 91-554-6568-4, 46 pp.

Ogata Y., 1983. Estimation of the parameters in the modified Omori formula for the aftershock frequencies by the maximum likelihood procedure. Journal of Physics Earth, 31, 115-124.

Öncel A.O., Main I., Alptekin Ö., Cowie, P., 1996. Spatial variations of the fractal properties of seismicity in the Anatolian fault zones. Tectonophysics, 257, 189-202.

Peresson H., Decker K., 1997. Far-field effects of Late Miocene subduction in the Eastern Carpatians: E-W compression and inversion of structures in the Alpine–Carpatian–Pannonian region. Tectonics, 16/1, 38-56.

Royden L.H., 1985. The Vienna Basin: a thin-skinned pull-apart basin. In: Biddle, K.T., Christie-Blick, N. (Eds.), Strike–slip deformation, basin formation and sedimentation: Society for Sedimentary Geology, Special Publication, 37, 319-338.

Schenková Z., Schenk V., Pospisil L., Kottnauer P., 1995. Seismogeological pattern of a transition area between the Eastern Alps and the Western Carpathians. Tectonophysics, 248, 235-245.

Scholz C. H., 1968. The frequency–magnitude relation of microfracturing in rock and its relation to earthquakes. Bulletin of Seismological Society of America, 58, 399-415.

Scholz C.H., 2002. The Mechanics of Earthquakes and Faulting. 2nd Edition. Cambridge University Press, Cambridge, 471 pp.

Scholz C.H., 2015. On the stress dependence of the earthquake b value. Geophysical Research Letters, 42, 1399-1402.

Schorlemmer D., Wiemer S., 2004. Earthquake statistics at Parkfield: 1. Stationarity of b values. Journal of Geophysical Research, 109, B12307. doi:10.1029/2004JB003234

Schorlemmer D., Wiemer S., 2005. Microseismicity data forecast rupture area. Nature, 434, 1086.

Sefara J., Kovac M., Plasienka D., Sujan M., 1998. Seismogenic zones in the Eastern Alpine–Western Carpathian–Pannonian junction area. Geologica Carpathica 49/4, 247-260.

Senatorski P., 2019. Gutenberg–Richter's b Value and Earthquake Asperity Models. Pure and applied Geophysics, 177, 1891-1905. doi:10.1007/s00024-019-02385-z

Shearer P., Stark P., 2011. Global risk of big earthquakes has not recently increased. Proceeding of the National Academy of Sciences, 109, 717-721. doi:10.1073/pnas.1118525109

Stein S., Liu M., 2009. Long aftershock sequences within continents and implications for earthquake hazard assessment. Nature, 462/5, 87-89. doi:10.1038/nature08502

Stepp J.C., 1972. Analysis of completeness of earthquake sample in the Puget Sound area and its effect on statistical estimates of earthquake hazard. National Oceanic and Atmospheric Administration Environmental Research Laboratories. Boulder Colorado, 80302.

Umnig E., Brückl E., Maras J., Weber R., 2015. Monitoring tectonic processes in Eastern Austria based on GNSS-derived site velocities. Vermessung & Geoinformation 2+3/2015, 198-207.

Wells D.L., Coppersmith K. J., 1994. New empirical relationship among magnitude rupture length, rupture width, rupture area, and surface displacement. Bulletin of Seismological Society of America, 84, 974-1002.

Wessely G., 1988. Structure and development of the Vienna basin in Austria. In: Royden L.H., Horváth F. (eds.), American Association of Petroleum Geologists, Memoir 45, 333-346.

Woessner J., Wiemer S., 2005. Assessing the quality of earthquake catalogues: Estimating the magnitude of completeness and its uncertainty. Bulletin of the Seismological Society of America, 95, 684-698. doi:10.1785/0120040007

ZAMG, 2020. Earthquake catalogue of felt earthquakes 1200– 2020 AD. (Austria). Computer File. Central Institute of Meteorology and Geodynamics (ZAMG), Vienna, Austria.

Received: 01.03.2022
Accepted: 28.01.2023
Editorial Handling: Walter Kurz